NISTIR 5767

Effect of Inclination on the Performance of a Compact Brazed Plate Condenser and Evaporator

Mark A. Kedzierski

November 1995

U.S. Department of Commerce
Ronald H. Brown, *Secretary*
Technology Administration
Mary L. Good, *Under Secretary for Technology*
National Institute of Standards and Technology
Arati Prabhakar, *Director*

Prepared for:
The Trane Company
Commercial Systems Division
3600 Pammel Creek Road
La Crosse, WI 54601-7599

ABSTRACT

This study experimentally quantified the performance change associated with tilting a compact brazed plate heat exchanger from the intended vertical position. Both clockwise and counterclockwise rotations within a plane perpendicular to the fittings were examined. A SWEP B15x36 was tested as an R-22 evaporator and condenser under fixed refrigerant state conditions suitable to high-efficiency water source heat pumps. This study showed that a substantial performance penalty occurred when the evaporator was rotated past 30° from the vertical. The evaporator capacity in the horizontal position was 62 to 74% of the vertical value. For a rotation angle of 30°, the degraded performance was within 5% of the vertical value. Rotation direction and entering refrigerant state had little effect on the performance of the evaporator for rotation angles less than 60°. Only when the evaporator was rotated to the horizontal position did rotation direction and refrigerant state have much effect. At the horizontal position, a subcooled-entering refrigerant and a counterclockwise rotation both tended to lessen the evaporator capacity degradation. Rotation of the condenser to the horizontal position improved the overall heat transfer coefficient by approximately 25%. Rotation direction had a negligible effect on the performance of the condenser.

TABLE OF CONTENTS

Abstract iii

Nomenclature v

Introduction 1

Test Apparatus 1

Test Results 3

Discussion 5

Conclusions 5

Acknowledgements 7

References 8

Appendix A 9

Appendix B 12

Tables 13

Figures 18

NOMENCLATURE

English symbols

ccw	counterclockwise
c_p	specific heat (kJ/kg•K)
cw	clockwise
$\dot{m}$	mass flow rate (kg/s)
q	test heat exchanger capacity (W)
T	temperature (K)
UA	overall conductance (W/K)
u_c	combined standard uncertainty

Greek symbols

$\Delta\bar{T}$	composite log-mean temperature difference (K)
ω	angle of rotation from the vertical (degrees)

subscripts

c	condenser
e	evaporator
i	inlet
l	liquid refrigerant
o	outlet
r	refrigerant
v	refrigerant vapor
w	water
2ϕ	two phase refrigerant
0	vertical position

INTRODUCTION

The origins of the compact brazed plate heat exchanger (CBE) began in the 1920's with the first commercially successful gasketed-plate heat exchangers (Saunders, 1988). Milk producers and other food and drink processors satisfied hygiene requirements by periodically disassembling and cleaning the gasketed-plates. The convenience of disassemblage limits the application of gasketed-plate heat exchangers to relative low pressure duties. By contrast, the CBE can sustain relatively large operating pressures because the edges of its plates are brazed together.

Applications for the compact brazed plate heat exchangers (CBEs) have increased in recent years. Currently, the compactness of the CBE drives its use as refrigerant evaporators and condensers. For example, Saunders (1988) cites a case where one CBE replaced several shell-and-tube heat exchangers. Consequently, research demonstrating the use of CBEs in refrigeration applications, like that of Carter et al. (1992), and Jonsson (1985), is becoming more prevalent. The accelerated application of CBEs to refrigerant equipment is sustained by pertinent design information. Unfortunately, the available research on CBEs as refrigerant evaporators and condensers is not entirely comprehensive.

No work was found in the open literature on the influence of gravity on the heat transfer performance of a CBE. Much of the work towards developing the means to predict the capacity of plate heat exchangers has focused on single phase heat transfer (Saniei and Dini (1993), Tinaut et al. (1992), and Kumar (1984)) where gravity effects should be insignificant. Also, two-phase studies with CBEs, such as that by Wang and Zhao (1993), remove the gravity effect by assuming a vertical installation. Intuitively, gravity should significantly affect the flow patterns in the narrow channels of a CBE. Consequently, tilting a CBE should affect the two-phase heat transfer.

The purpose of this study was to quantify the performance degradation associated with tilting a CBE from the designed vertical position. It may be advantageous to install the CBE skewed in equipment to achieve a cheaper and lower profile unit enclosure. A SWEP B15x36 was tested under operating conditions experienced by a evaporator and a condenser of a high-efficiency water source heat pump. The B15X36 contained thirty-six 466 mm x 72 mm stainless steel plates with a ridged herringbone pattern. The plates were stacked alternating the orientation of the herringbone pattern and then brazed with copper. When viewed in the vertical position, the CBE had 19 mm NPT connections located on the right front for the water stream and 22 mm solder connections on the left front for the refrigerant stream.

Figure 1 illustrates the orientation of the test heat exchanger as it is rotated clockwise and counterclockwise about an axis perpendicular to and centered on the front of the heat exchanger. Brazed plate heat exchangers have pointers stamped on the surface at one end which manufacturers recommend to point upward when installed (SWEP, 1992). Figures 1a and 1c show the evaporator and the condenser in the recommended vertical orientation, respectively. The fluid connections are located at the corners of the heat exchanger and extend outward from its face. The fluid streams of both the evaporator and the condenser are in counterflow. The refrigerant flows vertically up in the evaporator and down in the condenser. The heat exchanger is rotated about an axis centered on its face and parallel to the axis of the connections. The angle of rotation is measured from the vertical position.

TEST APPARATUS

Figure 2 shows a schematic of the test rig used to test the brazed plate heat exchanger. The main components of the rig are labeled on the figure as: (1) subcooler, (2) refrigerant pump, (3) de-subcooler,

(4) pre-evaporator, (5) reservoir/liquid desuperheater, (6) test heat exchanger, and (7) condensers. The de-subcooler was bypassed during the evaporation tests. The different refrigerant paths for evaporator and condenser tests are illustrated in Fig. 2.

The de-subcooler was operated and the desuperheater was disabled during the condensation tests. The purpose of the de-subcooler was to remove the subcooling. The subcooling prevented cavitation in the pump. The phase change occurred in the pre-evaporator where the saturation pressure was more readily controlled when the evaporator had little subcooling to remove. The refrigerant charge was reduced enough to keep liquid out of the desuperheater. Otherwise, saturated liquid would have entered the test section. Superheated vapor traveled from the pre-evaporator to the test condenser. The test condenser condensed the refrigerant which then bypassed the brine-cooled condensers and traveled to the subcooler to complete the loop.

The de-subcooler was bypassed and the desuperheater was operated during the evaporation tests. For the evaporator tests, the refrigerant exited the pre-evaporator as saturated liquid at approximately 1% thermodynamic quality. The low quality liquid-vapor mixture entered the top of the liquid desuperheater and exited the bottom as saturated liquid. The system charge was adjusted to keep liquid refrigerant in the bottom of the desuperheater. The refrigerant leaving the desuperheater entered the test evaporator. The test evaporator superheated the refrigerant to approximately 5.5 K above the saturation temperature. The refrigerant circuit was completed by the condensation of the superheated vapor in the condensers.

The loop contained all brazed plate heat exchangers except for the brine cooled condensers which were aluminum spiral heat exchangers. Brine at 260 K and 0.24 kg/s subcooled and condensed the test refrigerant in the subcooler and condensers, respectively. The mass flow rate of the subcooled refrigerant measured with the coriolis meter and that measured with the turbine meter always agreed within 1%.

Figure 2 illustrates the location of all the measurement devices. The subcooled liquid refrigerant temperatures were measured at the turbine meter and in the line between the de-subcooler and the pre-evaporator. The refrigerant pressure was also measured in the line between the de-subcooler and the pre-evaporator to determine the degree of subcooling there. The refrigerant temperatures were also measured in line at the entrance and exit of the test heat exchanger, along with the pressure drop across its inlet and exit. The absolute pressure of the refrigerant was measured at the inlet of the test heat exchanger.

Ten element thermopiles were used to measure the water temperature drop of the test heat exchanger and the pre-evaporator. The separate water flow rates for the test heat exchanger and the pre-evaporator were measured with turbine meters to calculate the capacity of each. The heat load of the pre-evaporator was used to calculate the inlet quality of the test heat exchanger. The heat load of the test heat exchanger was the focal point of this study and was also used to calculate its exit quality.

The capacity of the test heat exchanger, the measured refrigerant temperatures, and saturation pressure were used to calculate the average temperature difference between the water and refrigerant streams ($\Delta\overline{T}$) of the test heat exchanger as:

$$\Delta\overline{T} = \frac{q_v \, \Delta T_v + q_{2\phi} \, \Delta T_{2\phi} + q_l \, \Delta T_l}{q_T} \tag{1}$$

where the equations used to calculate the average temperature difference between: the water and refrigerant vapor (ΔT_v), water and two-phase refrigerant ($\Delta T_{2\phi}$), and water and refrigerant liquid (ΔT_l)

are given in Appendix A. Appendix B provides the equations used to calculate the vapor (q_v), two-phase ($q_{2\phi}$), and liquid (q_l) components of heat.

The overall conductance (UA) of the test heat exchanger was calculated as:

$$UA = \frac{q_T}{\Delta \overline{T}} \tag{2}$$

The estimated combined standard uncertainty (u_c) of the UA calculation, along with all other measurement u_c's, are presented in Table 1. The u_c is commonly referred to as the law of propagation of uncertainty.

The target operating conditions given in Tables 2 and 3 are applicable to those for current high-efficiency water source heat pump evaporators and condensers, respectively. Due to the limitations of water and brine flow rates and temperatures of the test loop, certain target conditions were unattainable. Consequently, the "as tested" conditions are given in Tables 2 and 3. Most of the evaporator target conditions were met. The refrigerant flow rate was marginally lower than the target value. The saturation temperature for the evaporator test was approximately 10 K greater than the target value. The condenser was tested at a saturation pressure lower than the target condition. Also, the refrigerant mass flow rate of the condenser was approximately half that of the target due to insufficient water flow to the condenser. It is believed that the observed relative performance with heat exchanger rotation should not be significantly different from that which would have been observed at the target conditions.

TEST RESULTS

The test results for the evaporator and the condenser are summarized in Tables 4 and 5, respectively. The tables provide the heat load, the overall conductance, the mean temperature difference, and the refrigerant flow rate averaged for each rotation angle. The R-22 saturation temperature, the inlet and exit thermodynamic state conditions of the refrigerant, the water flow rate, and the inlet water temperature were all fixed for both the condenser and evaporator tests.

Figures 3 through 9 present the data given in Tables 4 and 5 normalized by the data measured when the CBE was in the vertical position. The lines given in the graphs were obtained from a cubic regression on the rotation angle. Table 6 provides the magnitude of the average 95% confidence interval for the cubic regression. Following is a discussion of Figs. 3 through 9.

Evaporator

The test procedure for the evaporator was designed to simulate how an actual heat pump would react to a loss of evaporator capacity when the evaporator was tilted. The function of a thermostatic or electronic expansion valve in a heat pump is to adjust the refrigerant flow rate so that a desired superheat exits the evaporator. A loss of capacity causes the expansion valve to reduce the refrigerant flow rate to maintain a fixed evaporator superheat. Maintaining fixed exiting evaporator superheat while the evaporator capacity deteriorated was achieved by reducing the refrigerant pump speed in the present test loop.

Four different test sets were performed on the evaporator. The first two sets were for saturated entering refrigerant conditions; one test set was rotated clockwise, and the other test set was rotated counterclockwise. The last two test sets were for subcooled-entering refrigerant with the test heat

exchanger rotated clockwise and counterclockwise. The subcooled-entering refrigerant tests were used to investigate the effect of flow distribution on the performance of the evaporator. Engelhorn and Reinhart (1990) showed that flow maldistribution adversely affects the performance of a R-22 CBE evaporator. Also, Edwards et al. (1984) have experimentally shown that maldistribution of single phase flow is relatively insignificant for 20 plates. For a 40 plate CBE, Edwards et al. (1984) found that the mass flow in the first 24 plates and the last 16 plates was on average 8% below and 8% above a uniformly distributed flow, respectively. The present CBE contains 36 plates. Consequently, if the saturated entering flow is maldistributed, the subcooled-entering flow should exhibit a more uniform flow distribution and a smaller performance degradation. The amount of subcooling was set equal to the drop in saturation temperature that would have occurred for the entire pressure drop of the test heat exchanger. This criterion lessened the amount of flashing that occurred at the entrance and possibly eliminated it.

Figure 3 shows the normalized capacity of the evaporator as a function of inclination angle (ω). For a given test run, the data was normalized by the capacity measured at the vertical position (q_{e0}). The data illustrate that for rotation angles less than 60°, there is essentially no difference among clockwise, counterclockwise, saturated, or subcooled-entering conditions. For 30°, the evaporator performance is within 5% of the vertical (0°) value. For angles greater than 30°, the performance rapidly degrades. In the horizontal position (90°), the capacity is approximately 62 to 74% of the vertical position capacity. The performance degradation in the horizontal position depends on the refrigerant entering state and the rotation direction. Both subcooled-entering refrigerant and a counterclockwise rotation tended to minimize the performance degradation. This suggests that neither refrigerant flow distribution nor the relative position of the refrigerant and water connection have much affect on performance until the evaporator is nearly horizontal.

Figure 4 shows the refrigerant mass flow rate ($\dot{m}_e$) reduction required to maintain the 5.56 K (10 °F) exit evaporator superheat. As expected, the capacity loss is directly proportional to the refrigerant mass flow rate reduction. The severe deterioration of the mass flow rate does not occur until the heat exchanger is tilted past 30°.

Figures 5 and 6 show the normalized overall conductance (UA_e) and the composite log-mean temperature difference (ΔT_e) versus inclination angle (ω). The overall conductance of the evaporator decreased nearly linearly with evaporator rotation. The temperature difference increased linearly with evaporator rotation for angles greater than 30°. For angles less than 30°, the ΔT_e remained within 10% of the vertical value. Neither rotation direction nor entering-refrigerant condition affected the UA_e or the ΔT_e for angles less than 60°. When the evaporator was in the horizontal position, there was a small trend that was consistent with the evaporator heat load in the horizontal position. Both subcooled-entering refrigerant and a counterclockwise rotation tended to reduce UA_e and increase ΔT_e.

Condenser

Clockwise and counterclockwise rotation tests were performed on the condenser. Vapor superheated to 40 K above the saturation temperature entered the test brazed plate condenser. The condenser condensed the vapor and subsequently subcooled the liquid to approximately 8 K below the saturation temperature.

Figure 7 shows the normalized capacity of the condenser as a function of inclination angle (ω). For a given test run, the data was normalized by the capacity measured at the vertical position (q_{c0}). The data illustrate that neither rotation nor rotation direction have any effect on the condenser performance. The condenser performance is within 2% of the vertical (0°) value which is within the u_c of the capacity

measurement. Recall that the tests were conducted to meet a fixed condensing pressure and entering and leaving refrigerant temperatures. The operating conditions were achieved while the condenser refrigerant mass flow rate remained at approximately 0.029 kg/s for all tests. The ability of the condenser to satisfy the refrigerant state at a fixed refrigerant mass flow implies that it did not experience a heat transfer degradation with rotation.

Figures 8 and 9 show the overall conductance (UA_c) and the composite log-mean temperature difference (ΔT_c) versus inclination angle (ω). The figures show that the constant condenser load was met by an increasing UA_c and a decreasing ΔT_e. Both the UA_c and the ΔT_e behaved nearly linearly with rotation. The difference between counterclockwise and clockwise rotation was nearly within the u_c of the UA_c calculation. The overall conductance of the condenser in the horizontal position was approximately 25% greater than that for the vertical position. The ΔT_c in the horizontal position was approximately 20% smaller than that in the vertical position. The 20% reduction ΔT_c typically represented a reduction of less than 1 K. Overall, Figs. 8 and 9 show that installation of a CBE condenser in the horizontal position is more favorable for heat transfer than the vertical position.

DISCUSSION

Figure 10 shows the hypothesized liquid/vapor distribution within the heat exchanger for the evaporator and the condenser. The cross sectional flow area of the channels are simplified for ease of illustration. Nevertheless, the concepts for the overall liquid and vapor distributions should remain valid.

The evaporator suffers a degradation when tilted horizontally due to stratification of the flow. The stratified flow causes dryout of the upper surface of the channel and accumulation of liquid into thick films on the lower portion of the channel. Both dryout and thick liquid films cause poor heat transfer. The vertical position is favorable for flow boiling because the liquid film is distributed more evenly in an annular flow pattern. Consequently, the liquid film is thin and effective for heat transfer in annular flow.

Figure 10 also describes the mechanism responsible for the improvement of the overall heat transfer coefficient of the condenser when it is tilted in the horizontal position. The rotation changes the condensing length of the film. The condensing length is 72 mm and 466 mm long when the condenser is in the horizontal and vertical positions, respectively. The longer condensing length permits the film thickness to build. The thin film region near the leading edge of the condensing length exhibits the most favorable heat transfer. The length of the leading edge for the condenser in the horizontal position is nearly 6.5 times that for the condenser in the vertical position. Consequently, the average condensate film thickness for the condenser in the horizontal position is thinner than that in the vertical position. Thin condensate films induce a greater overall heat transfer coefficient for the condenser in the horizontal position.

CONCLUSIONS

Experimental investigation of the effect of inclination on the performance of a brazed plate heat exchanger revealed that a substantial performance penalty occurs for the evaporator as it is rotated past 30° from the vertical. The evaporator lost 62% to 74% of its capacity to maintain fixed refrigerant states when tilted to the horizontal position. Whereas, the condenser satisfied fixed refrigerant states without a loss in capacity when tilted. The overall heat transfer coefficient of the condenser improved by approximately 25% by rotating it to the horizontal position.

Rotation direction and entering-refrigerant state had little effect on the performance of the evaporator for rotation angles less than 60°. For a rotation angle of 30°, the performance degradation was within 5% of the vertical value. The evaporation degradation results from stratification of the flow into a dryout region and thick film region. Only when the evaporator was rotated to the full horizontal position did rotation direction and refrigerant state have much effect. At the horizontal position, a subcooled-entering refrigerant and a counterclockwise rotation both tended to minimize the performance degradation.

Rotation direction had little effect on the condenser performance. The overall heat transfer coefficient of the condenser improved nearly linearly with rotation. The results suggest that a compact braze heat exchanger performs best as a condenser when the width is installed in the vertical direction to give the shortest condensing length.

ACKNOWLEDGEMENTS

NIST and The Trane Company, under Project Manager Gary Lange, jointly funded this work. Thanks go to the following NIST and Trane personnel for their constructive criticism of the first draft of the manuscript: Dr. D. Didion, Mr. B. Dougherty, Mrs. J. Land, and Mr. G. Lange (Trane). The author would also like to express appreciation to Mr. A. Goelz and Mr. J. Sponsky for data collection.

REFERENCES

SWEP International AB, 1992, Compact Brazed Heat Exchangers for Refrigerant Applications, Technical Handbook.

Edwards, M. F., Ellis, D. I., and Amooie-Foumeny, M., 1984, "The Flow Distribution in Plate Heat Exchangers," First U.K. National Conference on Heat Transfer, Vol. 2, pp. 1289-1302.

Engelhorn, H. R. and Reinhart, A. M., 1990, "Investigations on Heat Transfer in a Plate Evaporator," Chem. Eng. Process, Vol. 28, pp. 143-146.

Falls, R. S., Carter, J. R., and Kavanaugh, S. P., 1992, "Test Results of a Water-to-air Heat Pump with a Brazed Plate Heat Exchanger for Ground-Coupled Applications, ASME-JSES-KSES Int. Sol. Energy Conf. Part 1, pp. 417-423.

Jonsson, I., 1985, "Plate Heat Exchangers as Evaporators and Condensers for Refrigerants," Australian Ref., Air Cond. and Heating, Vol. 39., No., 9, PP. 30-31.

Kumar, H., 1984, "The Plate Heat Exchanger: Construction and Design," First U.K. National Conference on Heat Transfer, Vol. 2, pp. 1275-1278.

Saniei, N. and Said, D., 1993, "Effect of Height and Geometry on Local Heat Transfer and Pressure Drop in a Channel with Corrugated Walls," Heat Transfer Engineering, Vol. 14, No. 4, pp. 19-31.

Saunders, E. A. D., 1988, Heat Exchangers Selection, Design and Construction, John Wiley & Sons, Inc., New York.

Tinaut, F. V., Melgar, A., and Rahman Ali, A. A., 1992, "Correlations for Heat Transfer and Flow Friction Characteristics of Compact Plate-Type Heat Exchangers," Int. J. Heat Mass Transfer, Vol. 35, No. 7, pp. 1659-1665.

Wang, Z. and Zhao, Z., 1993, "Analysis of Performance of Steam Condensation Heat Transfer and Pressure Drop in Plate Condensers," Heat Transfer Engineering, Vol. 14, No., 4, pp. 32-41.

APPENDIX A

This Appendix presents the equations that were used to calculate the average temperature difference between the water and the condensing refrigerant vapor (ΔT_v), between the water and the two-phase refrigerant ($\Delta T_{2\phi}$), and between the water and the refrigerant liquid (ΔT_l).

Evaporator

The average temperature between the refrigerant and water streams while the refrigerant was single phase vapor (ΔT_v) was calculated as:

$$\Delta T_v = \frac{(T_{r_o} - T_s)\left[\frac{\dot{m}_r c_{p_v}}{\dot{m}_w c_{p_w}} - 1\right]}{\ln \frac{T_{w_i} - T_{r_o}}{T_{w_b} - T_s}} \tag{3}$$

where $\dot{m}_r$ and $\dot{m}_w$ are the refrigerant and water mass flow rates, respectively. The cp_v and the cp_w are the specific heats of the refrigerant vapor and the water, respectively.

The average temperature difference between the water and the single phase refrigerant liquid was calculated from:

$$\Delta T_l = \frac{(T_{w_a} - T_s) - (T_{w_o} - T_{r_i})}{\ln \frac{(T_{w_a} - T_s)}{(T_{w_o} - T_{r_i})}} \tag{4}$$

where:

$$T_{w_a} = T_{w_o} + \frac{\dot{m}_r cp_l}{\dot{m}_w cp_w}(T_s - T_{r_i}) \tag{5}$$

The average temperature difference between the water and the two-phase refrigerant liquid was calculated from:

$$\Delta T_{2\phi} = \frac{T_{w_b} - T_{w_a}}{\ln\left[\frac{T_{w_b} - T_s}{T_{w_a} - T_s}\right]} \tag{6}$$

where:

$$T_{w_b} = T_{w_i} - \frac{\dot{m}_r cp_v}{\dot{m}_w cp_w} (T_{r_o} - T_s) \tag{7}$$

Condenser

The average temperature between the refrigerant and water streams while the refrigerant was single phase vapor (ΔT_v) was calculated as:

$$\Delta T_v = \frac{(T_{r_i} - T_s)\left[1 - \frac{\dot{m}_r cp_v}{\dot{m}_w cp_w}\right]}{\ln \frac{T_{r_i} - T_{w_o}}{T_s - T_{w_b}}} \tag{8}$$

where $\dot{m}_r$ and $\dot{m}_w$ are the refrigerant and water mass flow rates, respectively. The cp_v and the cp_w are the specific heats of the refrigerant vapor and the water, respectively.

The average temperature difference between the water and the single phase refrigerant liquid was calculated from:

$$\Delta T_l = \frac{(T_s - T_{w_a}) - (T_{r_o} - T_{w_i})}{\ln \frac{(T_s - T_{w_a})}{(T_{r_o} - T_{w_i})}} \tag{9}$$

where:

$$T_{w_a} = T_{w_i} + \frac{\dot{m}_r cp_l}{\dot{m}_w cp_w} (T_s - T_{r_o}) \tag{10}$$

The average temperature difference between the water and the two-phase refrigerant liquid was calculated from:

$$\Delta T_{2\phi} = \frac{T_{w_a} - T_{w_b}}{\ln\left(\frac{T_s - T_{w_b}}{T_s - T_{w_a}}\right)} \tag{11}$$

where:

$$T_{w_b} = T_{w_o} - \frac{\dot{m}_r cp_v}{\dot{m}_w cp_w} \left(T_{r_i} - T_s\right) \tag{12}$$

APPENDIX B

This Appendix presents the equations that were used to calculate the vapor, two-phase, and liquid components of heat: q_v, $q_{2\phi}$, and q_l, respectively.

The refrigerant vapor heat load for the condenser was calculated from:

$$q_{c_v} = \dot{m}_r c_{p_v} (T_{r_i} - T_s) \tag{13}$$

The refrigerant vapor heat load for the evaporator was calculated from:

$$q_{e_v} = \dot{m}_r c_{p_v} (T_s - T_{r_o}) \tag{14}$$

The refrigerant liquid heat load for the condenser was calculated from:

$$q_{c_l} = \dot{m}_r c_{p_l} (T_s - T_{r_o}) \tag{15}$$

The refrigerant liquid heat load for the evaporator was calculated from:

$$q_{e_l} = \dot{m}_r c_{p_l} (T_{r_i} - T_s) \tag{16}$$

The two-phase refrigerant heat load was calculated from:

$$q_{2\phi} = \dot{m}_w c_{p_w} |T_{w_o} - T_{w_i}| - q_v - q_l \tag{17}$$

Table 1 Combined Standard Measurement Uncertainties

Measured Parameter	u_c
Turbine ref. flow meter	±2% of the measured value
Coriolis ref. flow meter	±10E-4 kg/s
Absolute Temperature	0.2 K
Temperature Difference	0.01 K
Absolute ref. pressure	±2 kPa
Differential pressure	±0.26 kPa
Capacity test H-X	± 2%
UA of test H-X	± 3.4%
$\Delta\bar{T}$ (LMTD) of test H-X	± 3.8%

Table 2 Vertical Evaporator Operating Conditions

Operating Condition	Target	As Tested saturated inlet	As Tested subcooled inlet
refrigerant flow rate in vertical position	0.055 kg/s (433 lbm/hr)	0.051 kg/s (402 lbm/hr)	0.051 kg/s (402 lbm/hr)
refrigerant inlet temperature	280.37 K (45.0 °F)	290.7 K (63.59 °F)	289.8 K (61.97 °F)
saturated two phase	280.37 K (45.0 °F)	291.0 K (64.13 °F)	290.9 K (63.95 °F)
exit superheat	5.56 K (10 °F)	5.54 K (9.97 °F)	5.52 K (9.94 °F)
inlet water temperature	294.3 K (70 °F)	303.6 K (86.81 °F)	303.1 K (85.91 °F)
water flow rate	0.55 kg/s (8.75 GPM)	0.25 kg/s (3.98 GPM)	0.25 kg/s (3.98 GPM)

Table 3 Vertical Condenser Operating Conditions

Operating Condition	Target	As Tested (average)
refrigerant flow rate	0.06 kg/s (480 lbm/hr)	0.0285 kg/s
saturated condensing	311.8 K (101.6 °F)	292.7 K
refrigerant inlet temperature	347.0 K (165 °F)	349.6 K
subcooled exiting refrigerant temperature	303.7 K (101.6 °F)	284.6 K
entering water temperature	302.59 K (85 °F)	284.5 K
exiting water temperature	308.2 K (95 °F)	289.4 K
water flow rate	0.55 kg/s (8.75 GPM)	0.329 Kg/s

Table 4 Averaged Evaporator Data

ω (degrees)	q_e (W)	UA_e (W/K)	$\Delta\bar{T}$ (K)	$\dot{m}_r$ (kg/s)
Clockwise rotation, saturated inlet conditions				
0	10272	1435	7.16	0.051
30	9971	1252	7.97	0.050
45	9263	1011	9.17	0.046
60	8609	860	10.01	0.043
90	6379	479	13.34	0.033
Counterclockwise rotation, saturated inlet conditions				
0	10225	1451	7.05	0.051
30	10019	1274	7.87	0.050
45	9286	1060	8.77	0.046
60	8691	878	9.90	0.043
90	6742	521	12.95	0.036
Clockwise rotation, subcooled inlet conditions				
0	10225	1345	7.63	0.051
30	9875	1153	8.57	0.049
45	9151	936	9.79	0.046
60	8708	841	10.36	0.043
90	7010	516	13.60	0.038
Counterclockwise rotation, subcooled inlet conditions				
0	10251	1305	7.86	0.051
30	9883	1171	8.44	0.050
60	8749	781	11.20	0.044
90	7556	564	13.39	0.038

Table 5 Averaged Condenser Data

Clockwise rotation				
ω (degrees)	q_c (W)	UA_c (W/K)	$\Delta\bar{T}$ (K)	$\dot{m}_r$ (kg/s)
0	7092	944	7.52	0.029
20	7111	1004	7.09	0.029
30	7115	1049	6.81	0.029
45	7083	1098	6.53	0.029
60	7108	1154	6.21	0.029
75	7089	1204	5.98	0.029
90	7070	1114	6.35	0.029
Counterclockwise rotation				
0	6861	1646	4.18	0.028
20	6884	1823	3.82	0.028
30	6860	1941	3.54	0.028
45	6918	1993	3.47	0.028
60	6876	2067	3.35	0.028
75	6861	2168	3.19	0.028
90	6793	2183	3.13	0.028

Table 6 Average magnitude of 95% confidence interval for mean given in graphs

Test	UA/UA_o	q/q_o	$\Delta T/\Delta T_o$	$\dot{m}/\dot{m}_o$
Evaporator cw, saturated inlet	0.021	0.014	0.026	0.013
Evaporator ccw, saturated inlet	0.022	0.020	0.031	0.018
Evaporator cw, subcooled inlet	0.031	0.015	0.048	0.008
Evaporator ccw, subcooled inlet	0.038	0.014	0.040	0.008
Condenser cw	0.059	0.004	0.041	n/a
Condenser ccw	0.080	0.003	0.046	n/a

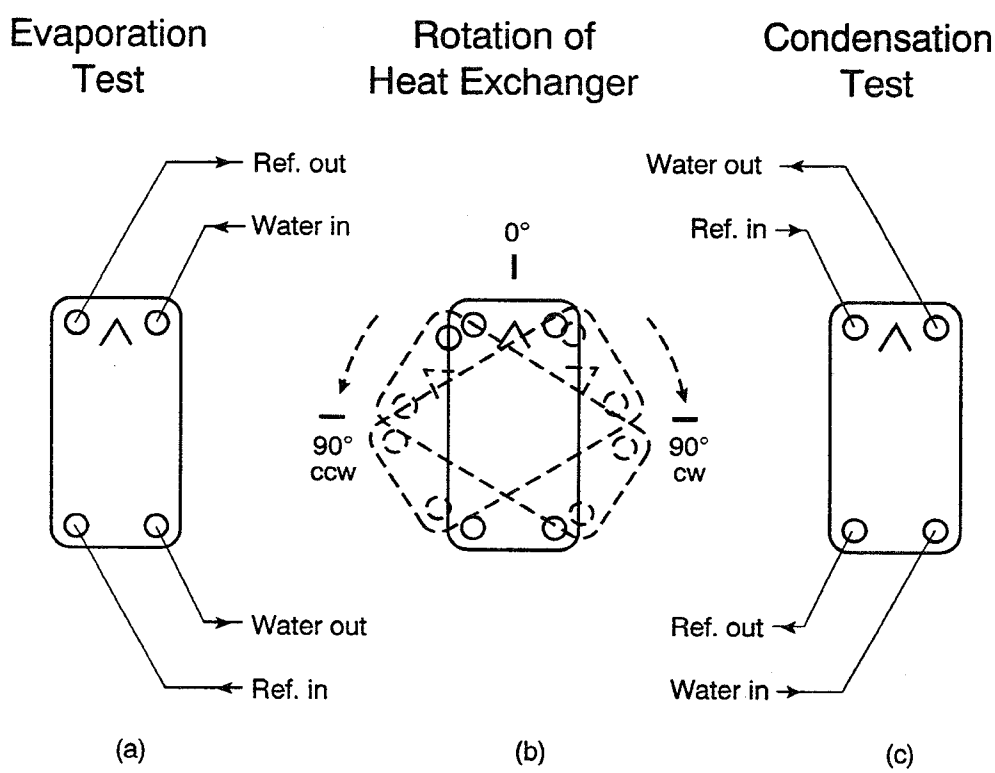

Fig. 1 Test heat exchanger orientation

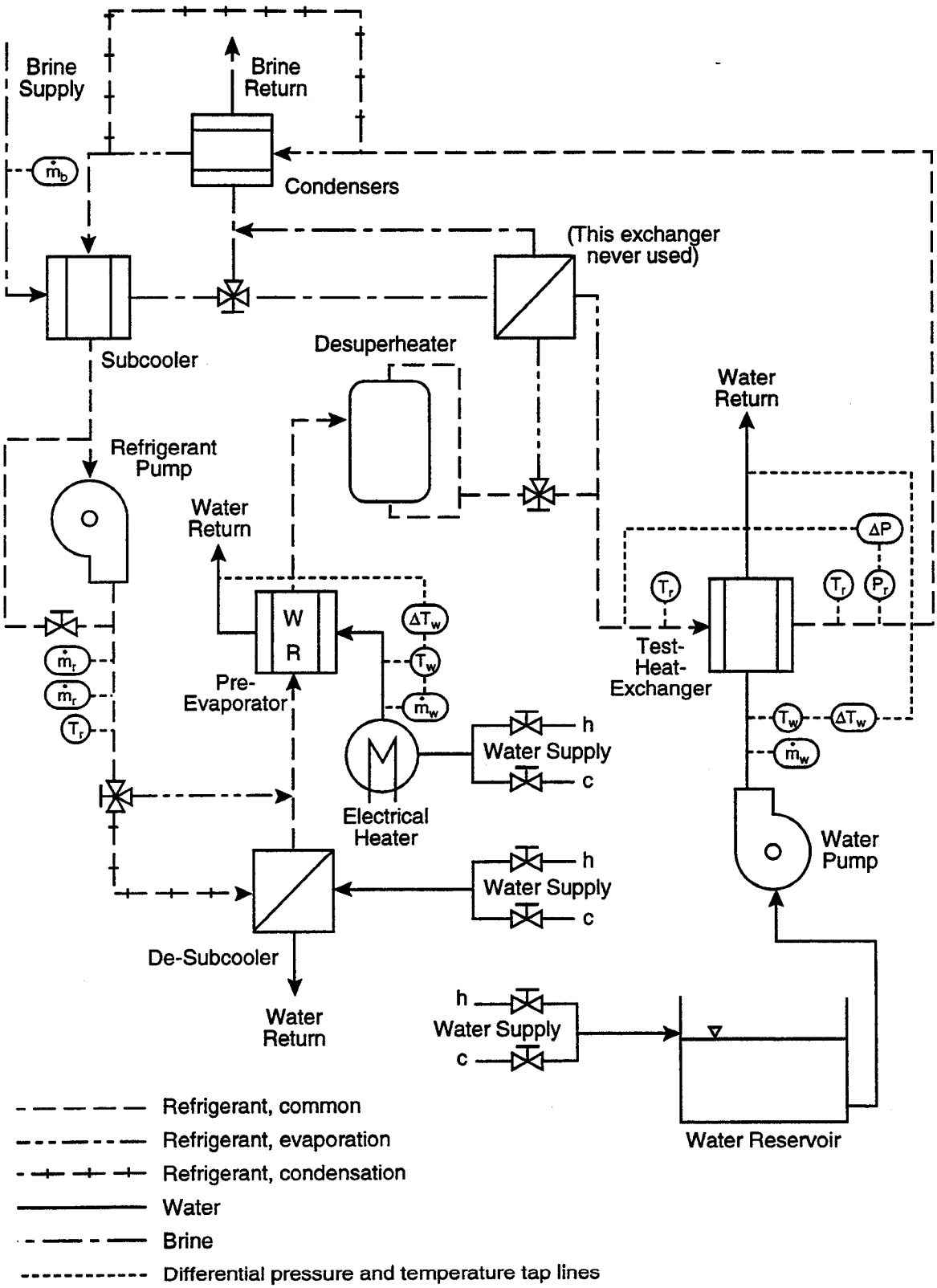

Fig. 2 Schematic of the test rig

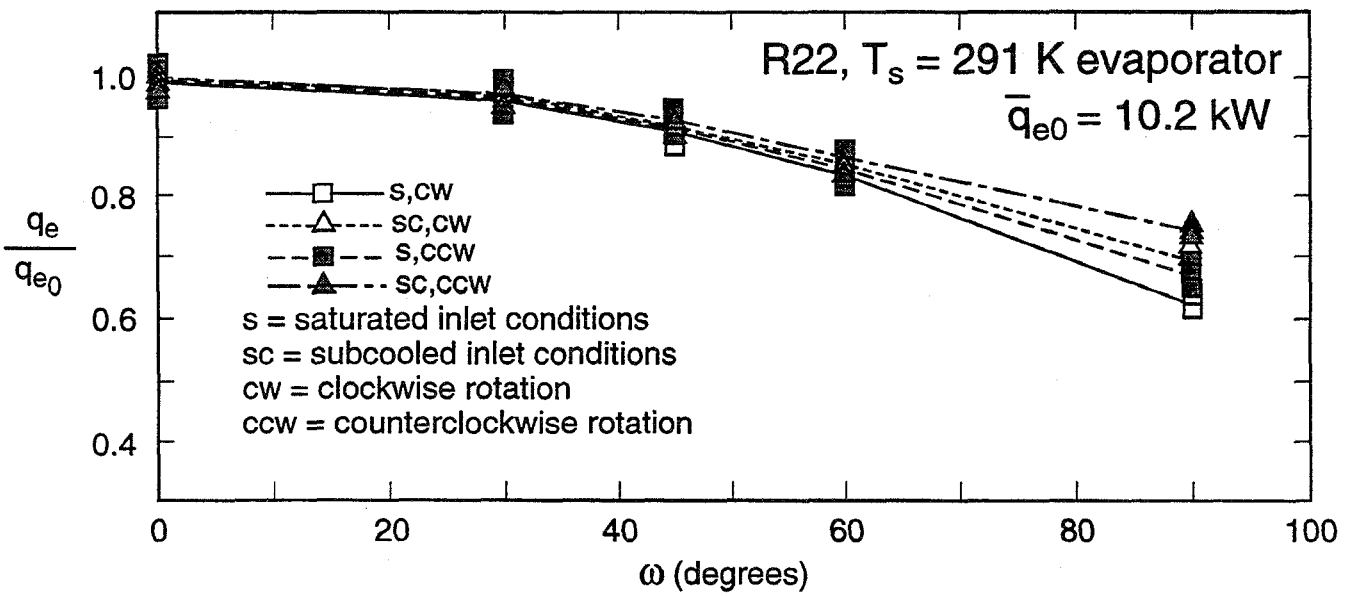

Fig. 3 Normalized capacity of the evaporator as a function of inclination angle

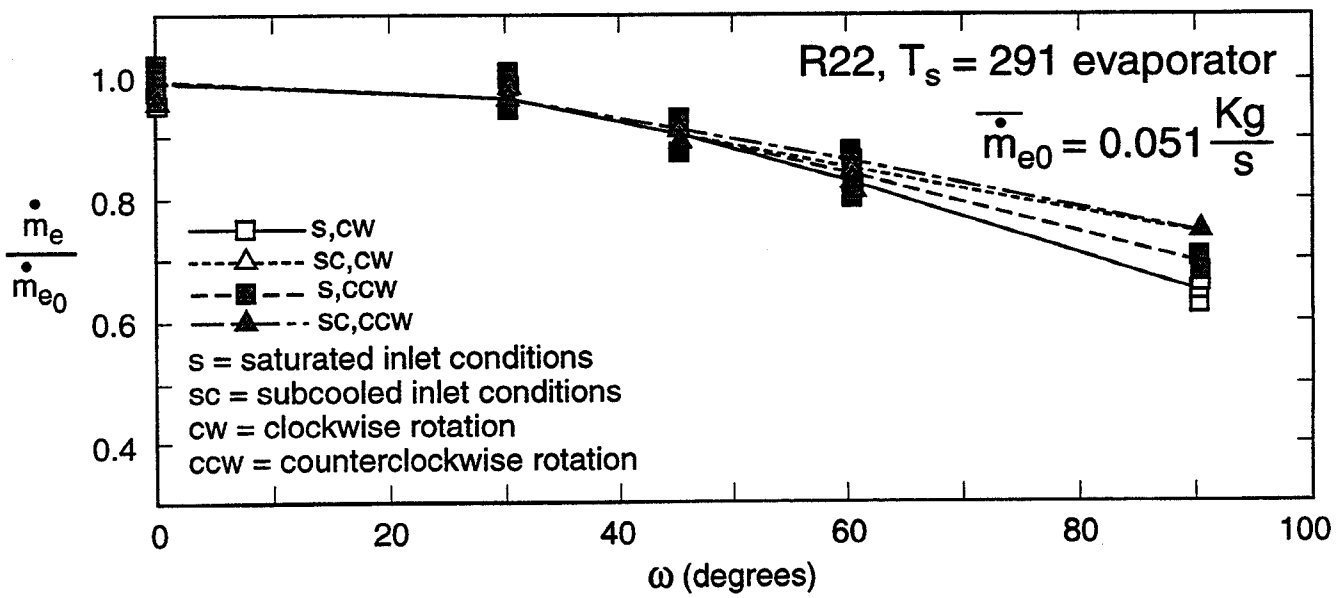

Fig. 4 Refrigerant mass flow rate reduction required to maintain the 5.56 K (10 °F) exit evaporator superheat

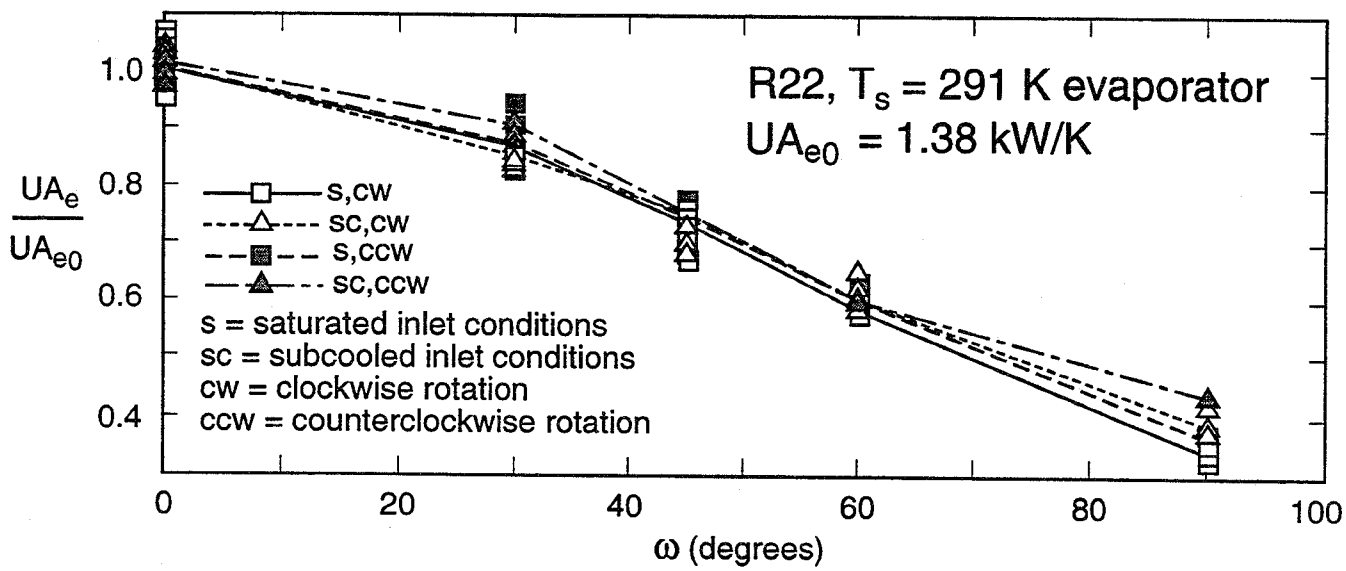

Fig. 5 Overall conductance versus inclination angle

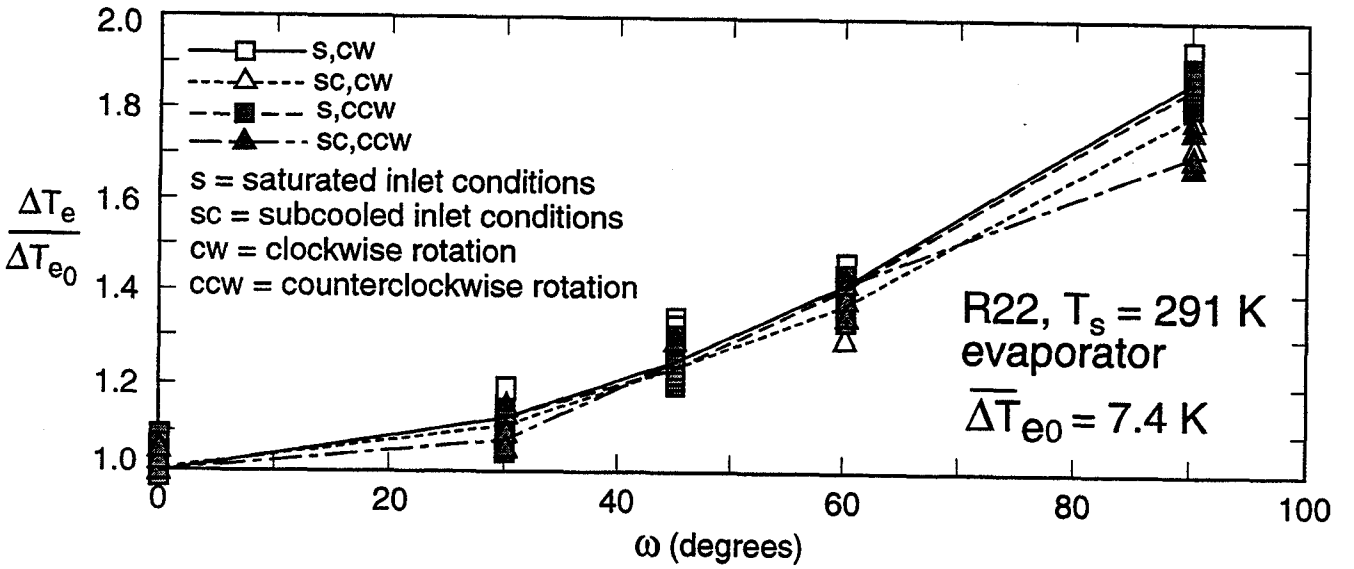

Fig. 6 Composite log-mean temperature difference of evaporator versus inclination angle

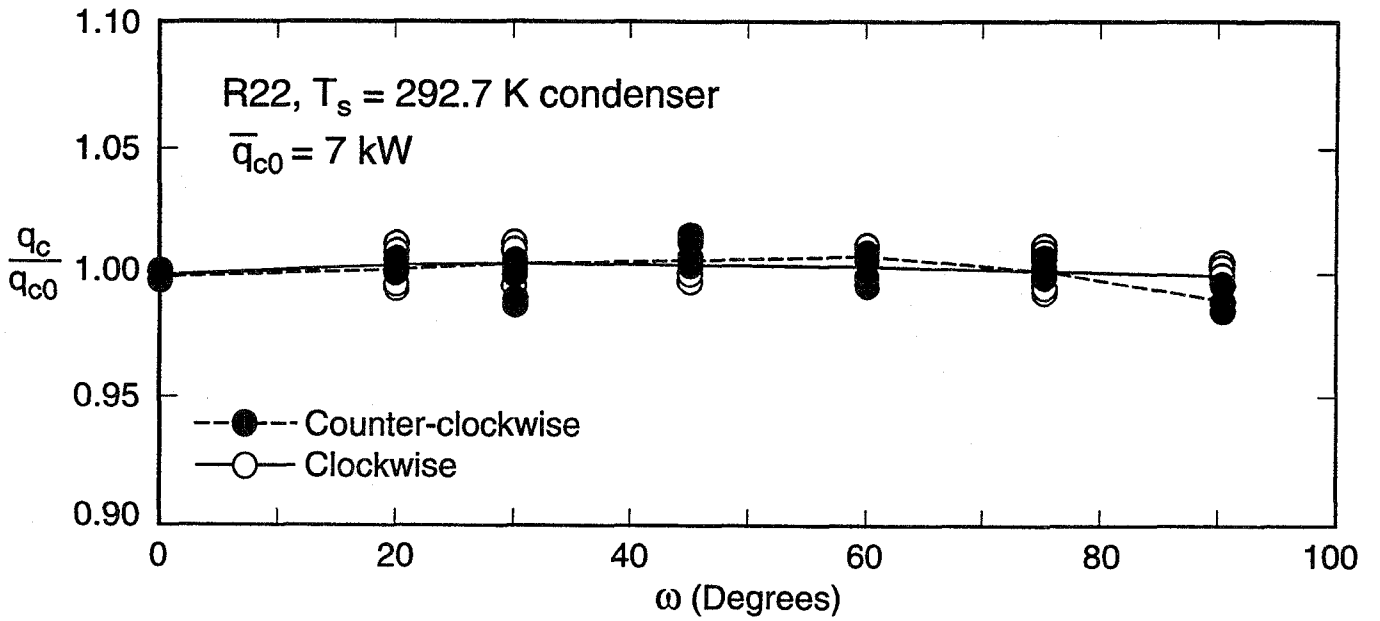

Fig. 7 Normalized capacity of the condenser as a function of inclination angle

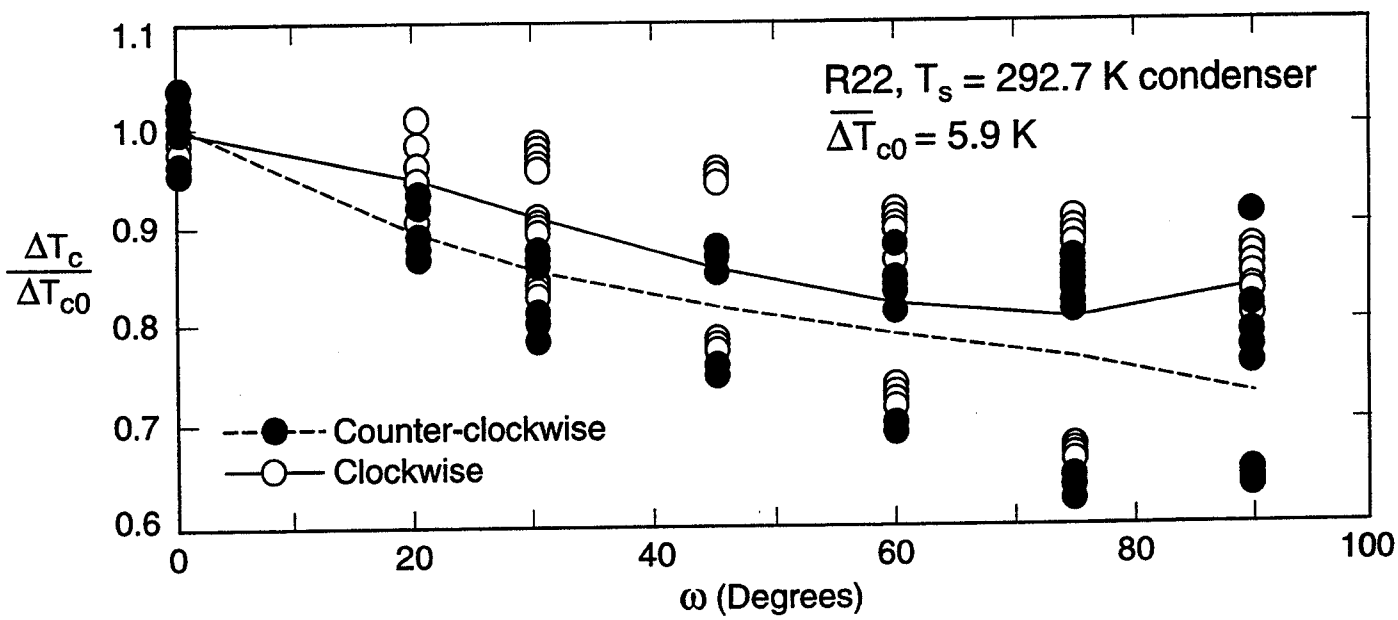

Fig. 8 Composite log-mean temperature difference of condenser versus inclination angle

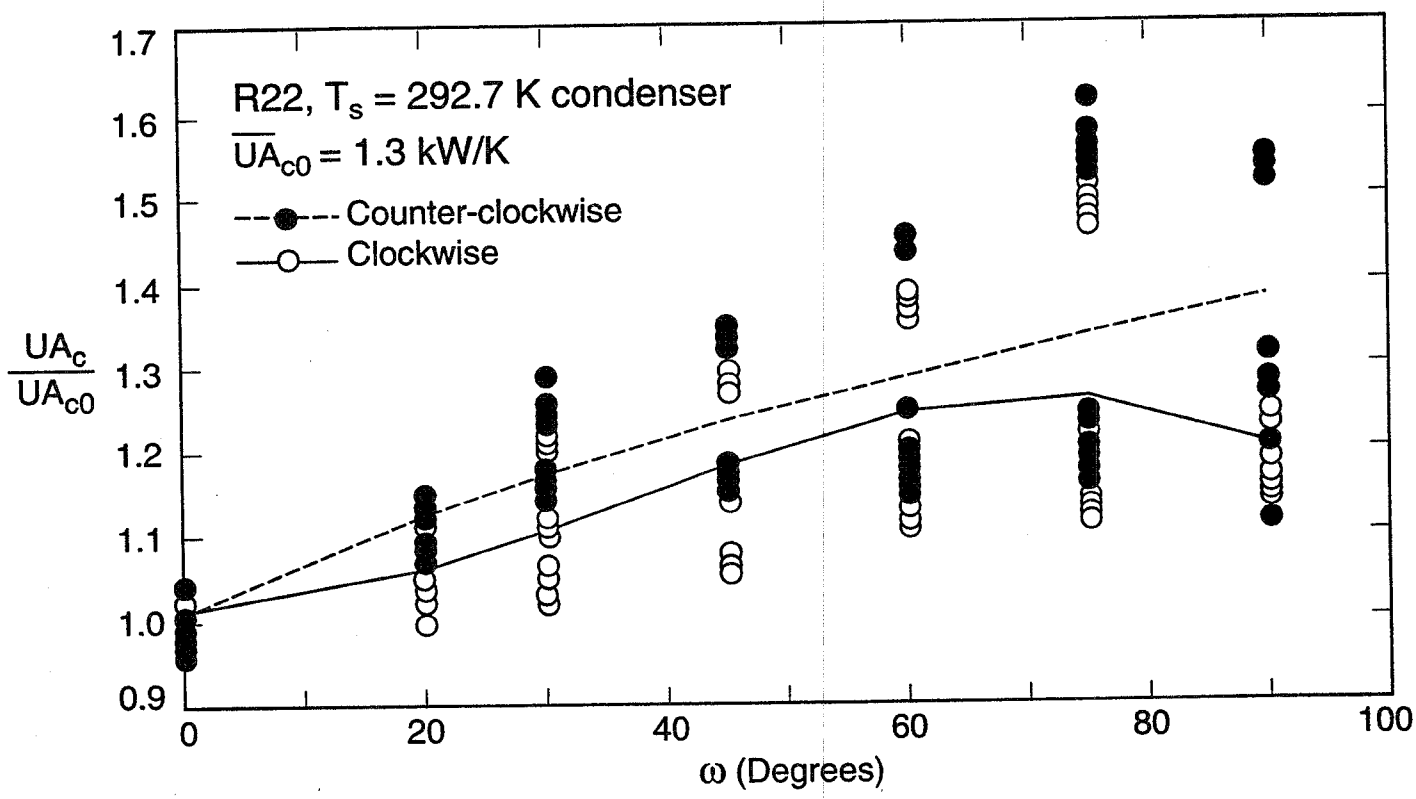

Fig. 9 Normalized overall conductance of the condenser as a function of inclination angle

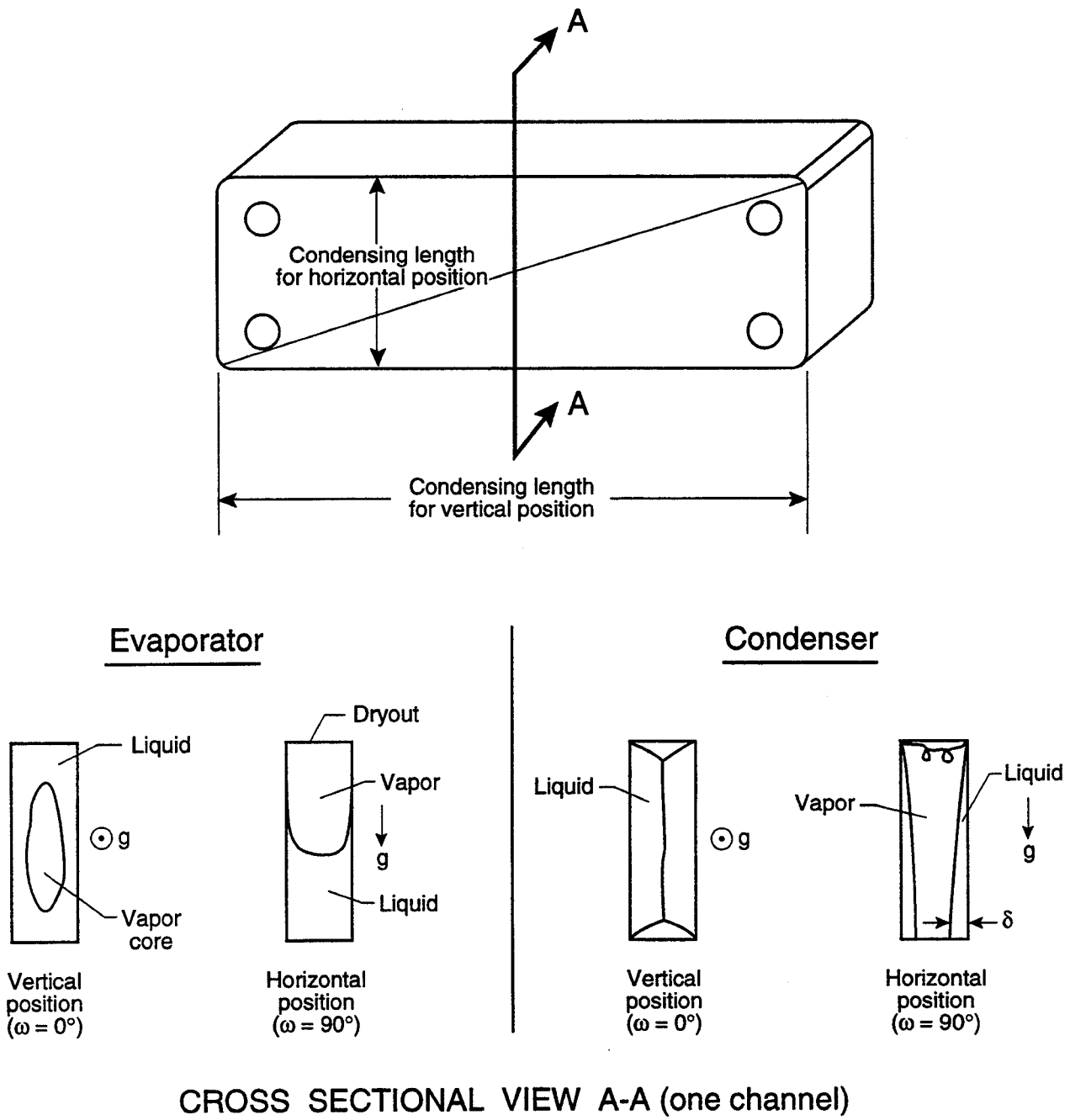

Fig. 10 Liquid/vapor distribution within the heat exchanger for the evaporator and the condenser